PAPER • OPEN ACCESS

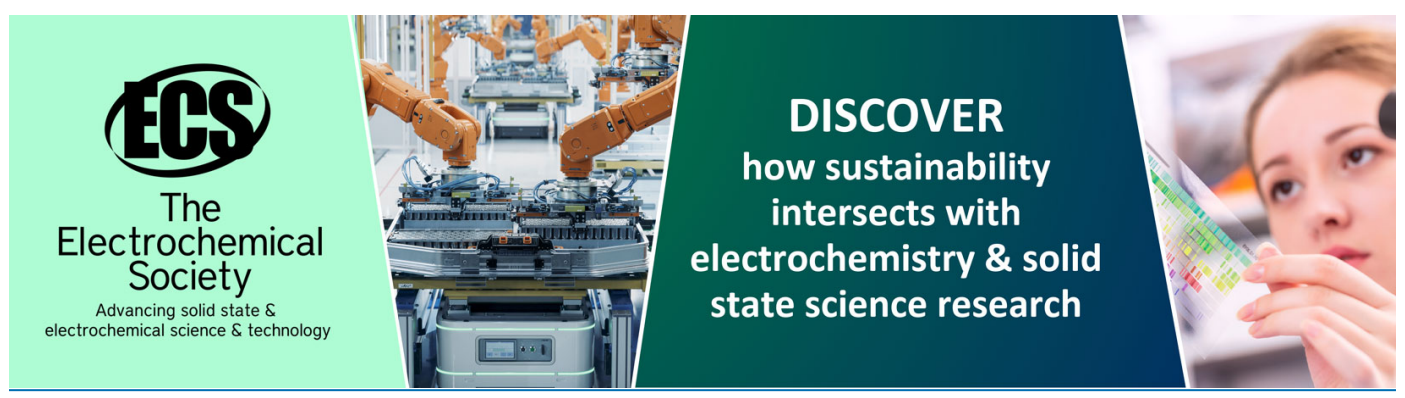
Modeling electron acceleration during the contraction of a magnetic island

To cite this article: Atit Deuja and Haihong Che 2024 J. Phys.: Conf. Ser. 2742 012015

View the <u>article online</u> for updates and enhancements.

You may also like

- Near-singular equilibrium currents near magnetic islands with broken symmetry
 A.H. Reiman and D. Radhakrishnan
- PARTICLE ACCELERATION VIA RECONNECTION PROCESSES IN THE SUPERSONIC SOLAR WIND G. P. Zank, J. A. Ie Roux, G. M. Webb et al.
- Bifurcation physics of magnetic islands and stochasticity explored by heat pulse propagation studies in toroidal plasmas K. Ida, T. Kobayashi, M. Yoshinuma et al.



2742 (2024) 012015

doi:10.1088/1742-6596/2742/1/012015

Modeling electron acceleration during the contraction of a magnetic island

Atit Deuja and Haihong Che

Center for Space Plasma and Aeronomic Research (CSPAR), University of Alabama in Huntsville, Huntsville, AL 35899, USA

Department of Space Science, University of Alabama in Huntsville, Huntsville, AL 35899, USA

E-mail: ad0159@uah.edu

Abstract. Magnetic reconnection releases the magnetic energy through the contraction of multi-magnetic island leading to the electron acceleration as proposed by Drake et. al in 2006. However, how the released magnetic energy is converted into electron's kinetic energy is still theoretically not well understood. We model in particular the kinetic process assuming the adiabatic contraction of magnetic island that induces electric field which is proportional to the vector potential of the magnetic island and approximate the magnetic island with an ellipse. Under this model, we show that the energy gain is achieved through the work of inductive electric field. We further show that the curvature drift which is along the inductive electric field dominates the energy gain. We compared our model with the magnetic island formed by tearing instability in a 2.5D particle-in-cell simulation of magnetic reconnection and found the results from the model consistent with that of the simulation.

1. Introduction

Particle acceleration is an essential phenomenon observed in various explosive events: for example, solar flares, magnetospheric substorms, gamma ray brusts, etc. in space [1, 2, 3], astrophysical [4, 5, 6] and also in laboratory [7, 8, 9] plasma. The magnetic reconnection (MR) is thought to be a major driver for these explosive events [10, 11, 12]. The MR is a fundamental plasma process that converts the magnetic energy into electromagnetic energy, heat and particle's kinetic energy via topological rearrangement of magnetic field lines.

In recent decades, extensive studies [8, 13, 14, 15, 16, 17, 18, 19, 20, 21, 22, 23, 24] have been carried out to understand the role of MR in particle acceleration within space and astrophysical plasmas. Specifically, the focus has been in understanding the processes involved in mildly relativistic particle acceleration during the events such as solar flares and magnetospheric substorms. But these studies posited an inherent challenge known as the "injection problem" [16], as the cosmic ray acceleration mechanism proposed by Fermi in 1949 necessitates preacceleration of particles to achieve a mildly relativistic speed for Fermi acceleration to occur [25]. The contraction of multi-magnetic island acceleration mechanism proposed by Drake [15] in 2006 is one of the commonly invoked model in solar flares. This mechanism suggests that during the contraction of multi-magnetic islands which are produced by tearing instability, electrons are accelerated during the bounce motion within the converging island and from the repetitive interaction among the randomly distributed magnetic islands. However, recent studies show

Content from this work may be used under the terms of the Creative Commons Attribution 3.0 licence. Any further distribution of this work must maintain attribution to the author(s) and the title of the work, journal citation and DOI.

2742 (2024) 012015

doi:10.1088/1742-6596/2742/1/012015

that the contraction of magnetic island is an adiabatic invariant process with particle exhibiting adiabatic motion [21, 26, 27]. The contraction timescale for a particle to exhibit such adiabatic motion requires it to be long and hence the acceleration process due to the contraction of magnetic island is a slow and inefficient process [19] in contrast to the Fermi acceleration which is a stochastic process.

It is yet unclear exactly what essential physical process governs the electron's motion in the contracting magnetic island and specifically whether the electron can achieve stochastic motion by the bouncing among the multiple magnetic islands. This requires the information of the time duration of electron confinement within a magnetic island, which is governed by the electron's interaction with the island. Recent studies [17, 21] based on fluid model and test particles showed that the curvature drift is a dominant source of electron heating but the underlying physics for the energy gain is still in question. In this paper, we aim to answer this question by presenting a model to grasp the essential physical process of the contracting magnetic island and then use test particles to study electron interaction with the islands. We compare the results from the model with the particle-in-cell (PIC) simulations to evaluate our model. The elongated magnetic island in the model is initially approximated by an ellipse, and assuming adiabatic contraction, the contracting magnetic island induces an electric field such that the curl of induced electric field is proportional to the magnetic field of the island. Under this model, the particle moving along the contracting magnetic island near the Alfven speed [15, 21] gets a kick intermediated by the induced electric field every time it passes through the ends of the magnetic island. We use test particle simulations to study particle motion, energy gain and drift velocities. The energy gain process in this scenario is dominated by curvature drift term where the electron gains energy through the work done by the induced electric field.

2. Modeling the contracting magnetic island

When the width of current sheets nears the ion inertial scale, the magnetic shear in current sheets leads to the onset of tearing instability [16] triggering the formation of multiple magnetic islands. The contraction of magnetic island is pictured by the gradual change in its geometry from elongated to a round due to the internal magnetic tension to relax the stored magnetic energy. The contraction of magnetic island is an adiabatic invariant process with the growth rate γ of the tearing instability being significantly smaller than the electron gyro-frequency Ω_e and the time scale Δt of one-cycle of electron motion along the magnetic island [28].

Figure 1 shows the schematic diagram of the contraction model of a two dimensional (2D) magnetic island. In the model, the elongated magnetic island is initially approximated by an ellipse in xy-plane which later contracts to form a circle releasing the magnetic energy where both the magnetic flux Φ and volume V remains approximately conserved for an in-compressible plasma with the radius of circle $r = \sqrt{ab}$ where a and b are the length of the semi-major and semi-minor axis of the ellipse.

The corresponding vector potential \mathbf{A}_z of the elongated 2D magnetic island approximated by an ellipse is given by,

$$\mathbf{A}_z = -d_i B_0 \left[\frac{(x - x_0)^2}{a^2} + \frac{(y - y_0)^2}{b^2} \right] \hat{\mathbf{z}}$$
 (1)

where d_i is the ion inertial length, B_0 is the asymptotic reconnection magnetic field, (x_0, y_0) is the center of the island, and a and b are respectively the length of semi-major and semi-minor axis. The magnetic field **B** is given by,

$$\mathbf{B} = \nabla \times \mathbf{A}_z = d_i B_0 \left[\frac{-2(y - y_0)}{b^2} \hat{\mathbf{x}} + \frac{2(x - x_0)}{a^2} \hat{\mathbf{y}} \right]$$
 (2)

2742 (2024) 012015

doi:10.1088/1742-6596/2742/1/012015

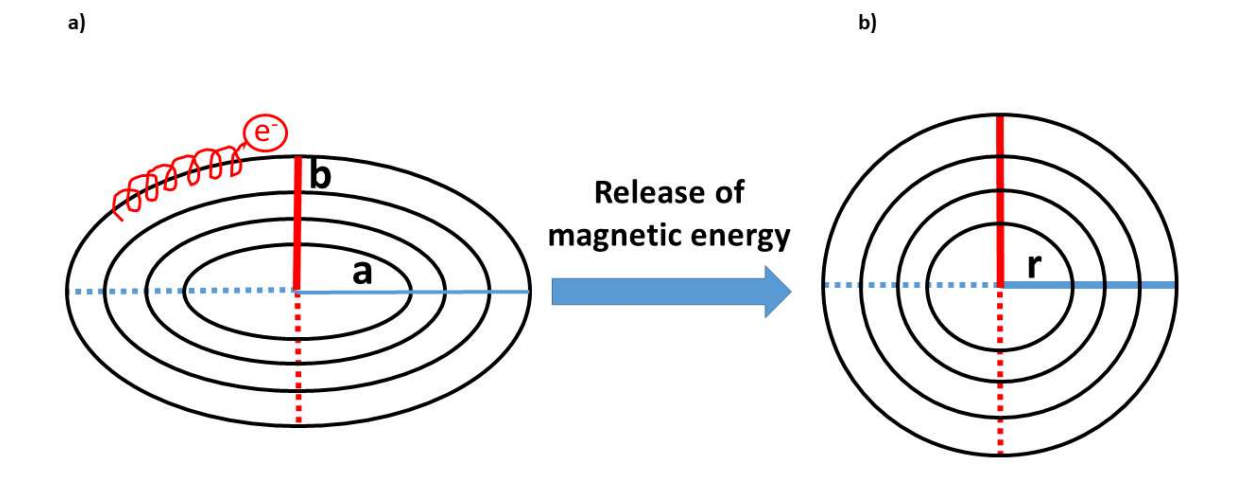


Figure 1. A schematic diagram of contraction model of a 2D elongated magnetic island described by equation (1). a) An elongated magnetic island contracts releasing magnetic energy and becomes b) a rounded magnetic island.

The current density \mathbf{J} can then be calculated as,

$$\mathbf{J} = \frac{c}{4\pi} \nabla \times \mathbf{B} = constant \tag{3}$$

where c is the speed of light. The slowly varying magnetic field induces electric field via Faraday's induction law i.e.

$$\nabla \times \mathbf{E}_{ind} = -\frac{1}{c} \frac{\partial \mathbf{B}}{\partial t} \tag{4}$$

Using equation 2, the induced electric field can be written as,

$$\mathbf{E}_{ind} = -\frac{1}{c} \frac{\partial \mathbf{A}_z}{\partial t} \tag{5}$$

We assume that the induced electric field is proportional to the vector potential,

$$\mathbf{E}_{ind} = C_R \frac{d_i B_0}{c} \left[\frac{(x - x_0)^2}{a^2} + \frac{(y - y_0)^2}{b^2} \right] \hat{\mathbf{z}}$$
 (6)

where C_R is a coefficient and the \mathbf{E}_{ind} is out-of-plane along z-axis. The current density calculated from the model is constant, which is not the case for a realistic magnetic island and hence it is a model's shortcoming. The model primarily emphasizes on the process of magnetic energy release through the contraction of magnetic island and acceleration of electrons via the inductive electric field, rather than exact MR process, which is better captured by the PIC simulation. Therefore, we extract the fundamental aspects of the contraction process and illustrate that the model effectively demonstrate the underlying physics, as we confirmed this through the comparison with the results from the PIC simulation.

2742 (2024) 012015

doi:10.1088/1742-6596/2742/1/012015

3. Simulations

To evaluate our model, we use the electric field **E** and magnetic field **B** data calculated from 2.5D PIC magnetic reconnection simulation using the p3d code [29]. The PIC simulation initializes from the doubly periodic two Harris current sheets with reconnection magnetic field configuration given by [15],

$$B_x = B_0 \left[\tanh\left(\frac{y - L_y/4}{w_0}\right) - \tanh\left(\frac{y - 3L_y/4}{w_0}\right) - 1 \right]$$
 (7)

where w_0 represents the half-thickness of the current sheets and L_y represents simulation domain length in y-directions. The simulation is carried out in the presence of a uniform guide field $B_q = 1.0B_0\hat{\mathbf{z}}$ and the particle density is given by [21],

$$n = n_0 \left[\operatorname{sech}^2 \left(\frac{y - L_y/4}{w_0} \right) + \operatorname{sech}^2 \left(\frac{y - 3L_y/4}{w_0} \right) \right]$$
 (8)

where n_0 is a peak density at the center of the current sheet superimposed over a uniform ambient density $0.2n_0$. The PIC code solves the relativistic Newton-Lorentz equations and Maxwell equations to trace particles' positions and trajectories in velocity space. In the simulation, the mass ratio used is $m_e/m_i=0.01$, the speed of light is $c=20v_A$ and the initial temperatures are set to $T_e/m_iv_A^2=1/12$ for electrons and $T_i/m_iv_A^2=5/12$ for ions, where m_e represents electron mass, m_i represents ion mass and $v_A=B_0/(4\pi n_0 m_i)^{1/2}$ denotes the Alfven speed. The simulation spatial dimensions are $L_x\times L_y=64d_i\times 32d_i$, where $d_i=c/(4\pi n_0 e^2/m_i)^{1/2}$ is the ion-inertial length with ion charge e, and consists of 4096×2048 cells. The boundary conditions used in the PIC simulation are periodic in both x and y-direction and the total simulation time used is $t=64.0\Omega_{ci}^{-1}$ with $\Omega_{ci}=eB_0/m_ic$.

We carried out 2.5D test particle simulations to investigate particle motion, energy gain and drift velocities in the magnetic islands, comparing results from both the model and PIC simulation. We solved the Newton-Lorentz equation to advance test particle and calculate its trajectory using Boris method [30]. We used an electron as a test particle with the same mass ratio $m_e/m_i = 0.01$ as in PIC simulation, and the charge q = -e. The electron injected into the simulation domain has the dimensions of $L_x \times L_y = 4d_i \times 2d_i$ that consists of 256 × 128 cells which is sufficient for the study of one single magnetic island. The spatial and temporal resolution in the test particle simulations are same to that of PIC simulation. The electron is treated under guiding center limit with a velocity \mathbf{v} given by;

$$\mathbf{v} = \mathbf{v}_{||} + \mathbf{v}_L + \mathbf{v}_E + \mathbf{v}_{cur} + \mathbf{v}_{\nabla B} \tag{9}$$

where the parallel velocity to the magnetic field $\mathbf{v}_{\parallel} = \mathbf{B}(\mathbf{v}.\mathbf{B})/B^2$, the Larmor velocity is \mathbf{v}_L , the $\mathbf{E} \times \mathbf{B}$ drift is,

$$\mathbf{v}_E = \frac{c\mathbf{E} \times \mathbf{B}}{B^2} \tag{10}$$

the gradient drift is,

$$\mathbf{v}_{\nabla B} = \frac{m_e v_\perp^2}{2q} \frac{c\mathbf{B} \times \nabla B}{B^3} \tag{11}$$

and the curvature drift is,

$$\mathbf{v}_{cur} = \frac{m_e v_{\parallel}^2}{a} \frac{c\mathbf{B} \times (\hat{\mathbf{b}}.\nabla)\hat{\mathbf{b}}}{B^2}$$
 (12)

respectively with the perpendicular velocity to the magnetic field $\mathbf{v}_{\perp} = \mathbf{v} - \mathbf{B}(\mathbf{v}.\mathbf{B})/B^2$. The particle drift \mathbf{v}_E acts along the xy-plane whereas the $\mathbf{v}_{\nabla B}$ and \mathbf{v}_{cur} drift is out-of-plane along z-axis.

2742 (2024) 012015 doi:10.1088/17-

doi:10.1088/1742-6596/2742/1/012015

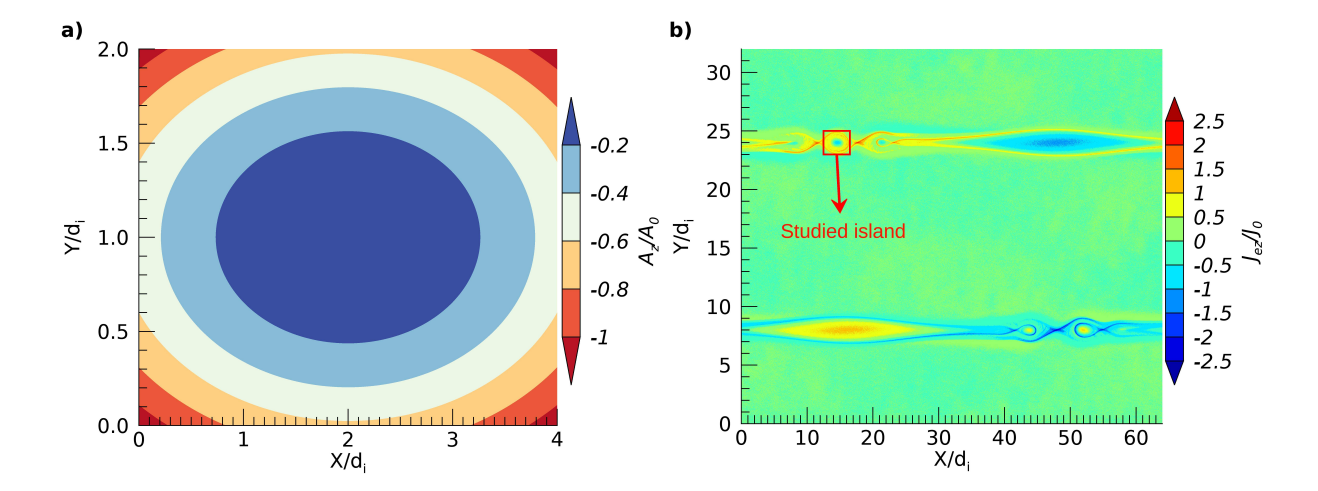


Figure 2. Contour of out-of-plane component of a) vector potential \mathbf{A}_z from the model with a=2.83 and b=1.26 and b) electron current density \mathbf{J}_{ez} from the PIC simulation at time $\Omega_{ci}t=19.8$ in the presence of the guide field $B_g=1.0B_0$. The highlighted square region (red) in b) denotes the studied magnetic island.

Table 1. Field description of test particle simulations

Name	Description
Model S1	$\mathbf{B} = (-2(y - y_0)/b^2, 2(x - x_0)/a^2, 0); \mathbf{E} = (0, 0, E_{ind})$ $\mathbf{B} = (B_x, B_y, 0); \mathbf{E} = (0, 0, E_z)$

To initialize the test particle simulation, length of semi-major axis a and semi-minor axis b of the ellipse approximating the magnetic island (as shown in figure 1) are chosen in such a way that the specification of the magnetic island in particular the magnetic field of the model closely matches to that of the studied magnetic island from the PIC simulation. Figure 2 shows the magnetic islands from (a) model and (b) PIC simulation. The magnetic island in the model is represented by an ellipse with dimension a=2.83 and b=1.26, centered at $(x_0,y_0)=(2,1)$. This specific choice of a and b generates magnetic field that scales close to the magnetic field configuration of the island marked by the solid red square in figure 2 (b). We present the contour plot of the out-of-plane vector potential \mathbf{A}_z normalized by the magnitude $A_0 = d_i B_0$ to analyze the modeled island in figure 2 (a) whose magnitude increases from center towards the edge of the island. Figure 2 (b) shows the contour of out-of-plane electron current density \mathbf{J}_{ez} obtained from the PIC simulation which dominates the current on kinetic scale. The studied magnetic island highlighted by the solid red square has domain size $L_x \times L_y = 4d_i \times 2d_i$ equal to that of modeled island which is also described in the xy-plane and consists 256×128 cells. The magnitude of the electron current density J_{ez} is expressed in the unit of $J_0 = n_0 e v_A$.

Table 1 shows the field description of the test particle simulations carried out in this study. The Model (in Table 1) describes the test particle simulation performed in magnetic island from the model whose field is given by equation 2 and equation 6. To evaluate our model, we performed a test particle simulation S1 under similar field conditions i.e. we take into account only x and y-components magnetic field data and out-of-plane electric field data from the PIC simulation.

2742 (2024) 012015 doi:10.1

doi:10.1088/1742-6596/2742/1/012015

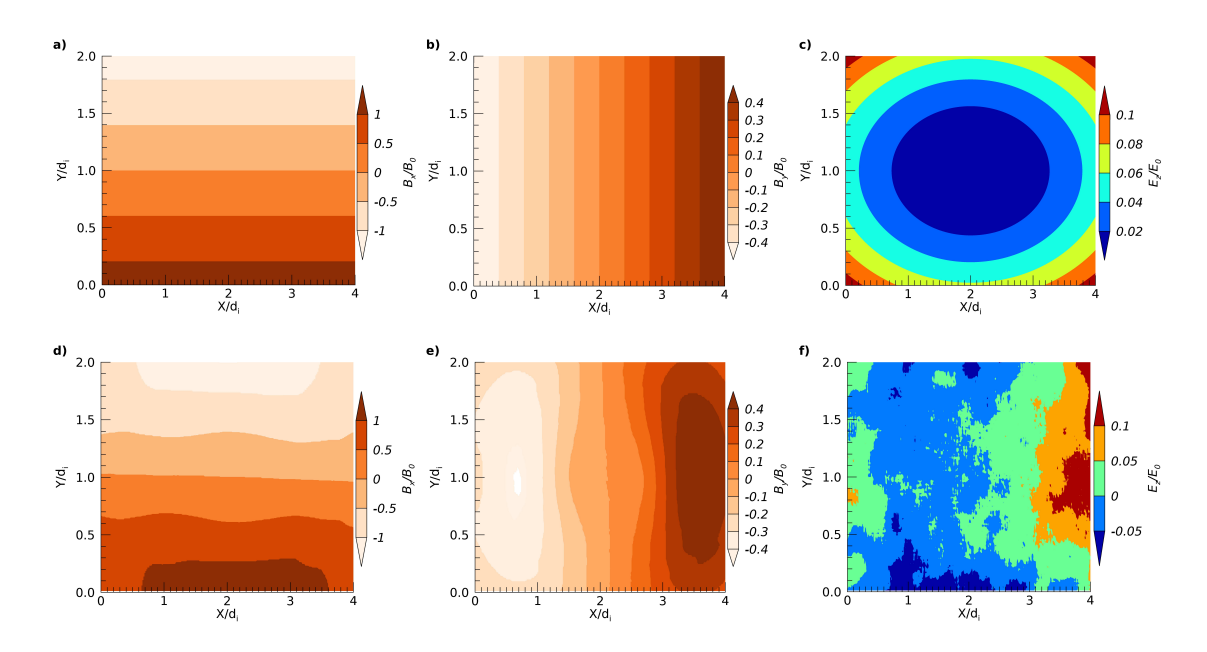


Figure 3. Top panel: a) x-component of the magnetic field \mathbf{B}_x , b) y-component of the magnetic field \mathbf{B}_y and c) out-of-plane electric field $\mathbf{E}_z = \mathbf{E}_{ind}$ with $C_R = 0.1$ from the model. Bottom panel: d) x-component of the magnetic field \mathbf{B}_x , e) y-component of the magnetic field \mathbf{B}_y and f) out-of-plane electric field \mathbf{E}_z from the PIC simulation.

4. Comparison of results from model and PIC simulation

Figure 3 shows the comparison of fields' components of elongated magnetic island from the model (top panel) with that of the studied island from the PIC simulation (bottom panel). The contours of magnetic field from the modeled magnetic island closely matches to that of the studied magnetic island from the PIC simulation. The x-component of the magnetic field ${\bf B}_x$ for both model and PIC simulation magnetic island (see figure 3 (a) and (d)), increases along the y-direction from the $y=y_0$ line on both sides and remains constant along the x-direction, whereas the y-component of the magnetic field \mathbf{B}_y (figure 3 (b) and (e)), increases along the x-direction from the $x = x_0$ line on both sides and remains constant along the y-direction. The near matching profiles of both the \mathbf{B}_x and \mathbf{B}_y -components of the modeled magnetic island compared to that of simulation island confirms the elliptic configuration of the magnetic island. Nevertheless, near at the edge of the simulation island, the magnetic field components experience distortion as a result of their interaction with its neighbouring magnetic islands. The induced electric field \mathbf{E}_{ind} (figure 3 (c)) from the model with a coefficient $C_R = 0.1$ is compared with the z-component of electric field \mathbf{E}_z from the PIC simulation. The magnitude of electric field is expressed in the unit of $E_0 = v_A B_0/c$. The model \mathbf{E}_{ind} is out-of-plane along positive z-direction whose magnitude increases from center to the edge of the magnetic island whereas the simulation \mathbf{E}_z is more complex with its field components align in both positive and negative direction. The color contour in figure 3 (f) shows that the positive field components dominates the \mathbf{E}_z , where the work is done by the mean electric field on electron velocity ${\bf v}$ and hence the electron gains energy for both the model and PIC simulation fields.

Figure 4 shows the comparison of electron trajectory, energy gain and the drift velocities calculated from the test particle simulation Model (top panel) with that of test particle simulation S1 (bottom panel). The electron's trajectory (red solid line in figure 4 (a)) is plotted in the background of induced electric field \mathbf{E}_{ind} (color contour) whereas the electron trajectory in

2742 (2024) 012015 doi:10.1088/1742-6596/2742/1/012015

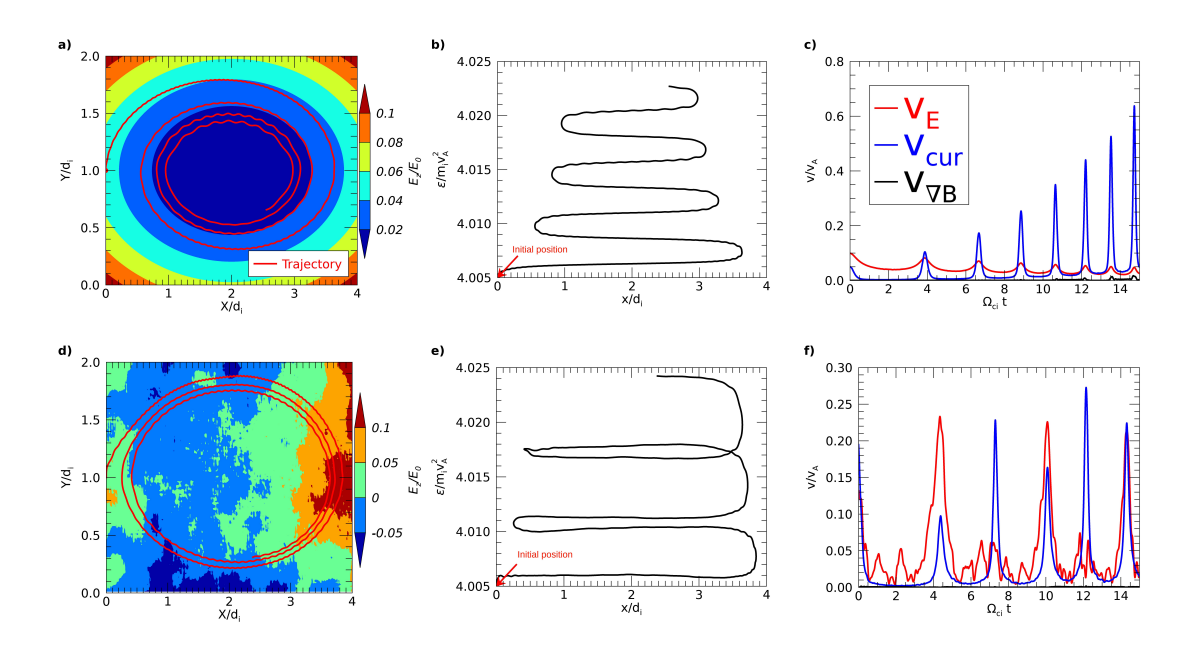


Figure 4. Top panel: a) Electron trajectory, b) energy gain and c) drift velocities calculated from the test particle simulation Model. Bottom panel: d) Electron trajectory, e) energy gain and f) drift velocities calculated from the test particle simulation S1.

figure 4 (d)) is plotted in the background of electric field \mathbf{E}_z (color contour). For a positive out-of-plane electric field, the electron moves along the magnetic field lines and slowly drifts inward into the magnetic island where it gains energy every time it bounces from the edge of the contracting magnetic island. Since the mean electric field \mathbf{E}_z in figure 4 (d) is positive, the electron trajectory for Model is consistent with that of S1. Electron's energy as a function of x position is shown in figure 4 (b) and figure 4(e). The electron's energy in figure 4 (b) remains nearly constant throughout the orbit but except at the edge where the curvature of the magnetic field is maximum, the electron gains energy through the work by the inductive electric field from the contracting magnetic island which is validated by figure 4 (e) obtained from the test particle simulation S1. Electron drift velocities evolution profile as a function of time is shown in figure 4 (c) and figure 4 (f). The magnitude of $\mathbf{E} \times \mathbf{B}$ drift v_E , curvature drift v_{cur} and gradient drift $v_{\nabla B}$ are respectively denoted by red, blue and black solid line. The curvature drift increases as the electron drift towards the center of the island and becomes a dominant since the magnitude of parallel velocity increases due to the acceleration of electron at the ends of the island by the induced electric field. On the other hand the v_E drift decreases as the magnitude of field components decreases along its trajectory. The gradient drift which depends upon the perpendicular energy of the electron (see figure 5) is very small compared to other drifts as the contraction of the magnetic island mostly affects parallel velocity of the electron.

Figure 5 shows that the magnetic moment μ and kinetic energy $k.\varepsilon$, evolution profile from the test particle simulations (a) Model and (b) S1. The μ is expressed in the unit of $\mu_0 = m_i v_A^2/B_0$ and the $k.\varepsilon$, is expressed in the unit of $m_i v_A^2$. For both Model and S1, the increase in total kinetic energy is mostly contributed by the increase in $k.\varepsilon$, due to parallel velocity. The magnitude of parallel velocity increases as the particle slowly drifts inward into the contracting magnetic island. The increase of parallel velocity is sharp at the ends of the magnetic island where the curvature of magnetic field strength is maximum and therefore the kinetic energy due to this parallel velocity increases sharply in this region. The magnetic moment μ for both Model and S1 remains nearly constant throughout the trajectory except at the ends where the Larmor velocity

2742 (2024) 012015 doi:10.1088/1742-6596/2742/1/012015

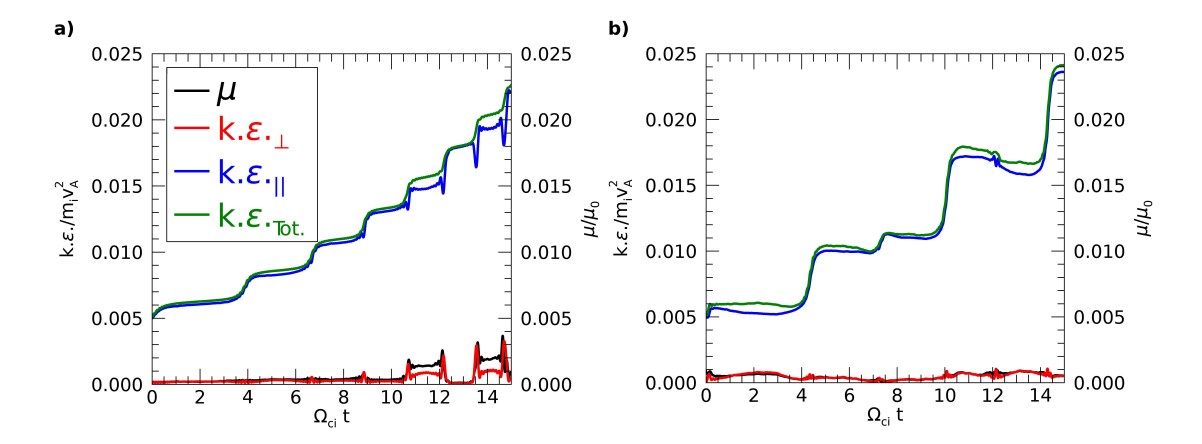


Figure 5. Magnetic moment and kinetic energy evolution profile from the test particle simulations a) Model and b) S1. The magnetic moment μ (black), kinetic energy due to perpendicular velocity $k.\varepsilon._{\perp}$ (red), kinetic energy due to parallel velocity $k.\varepsilon._{||}$ (blue) and the total kinetic energy $k.\varepsilon._{Tot.}$ are shown respectively in figures above.

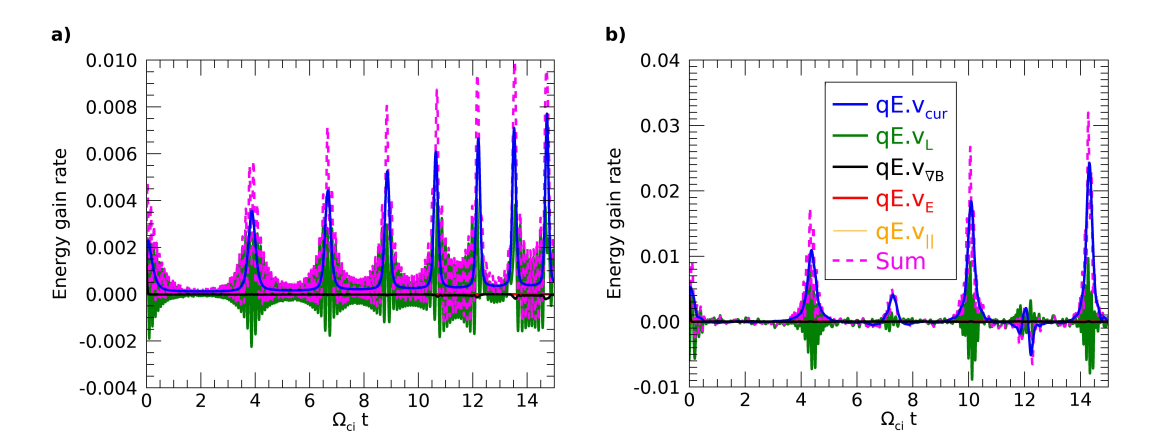


Figure 6. Electron's energy gain rate corresponding to the different velocity terms described by equation (13) from the test particle simulations a) Model and b) S1. The contributions of various velocity terms to energy gain, in descending order of their magnitude, are as follows: curvature drift (blue), Larmor velocity (green) and gradient drift (black). The $\mathbf{E} \times \mathbf{B}$ drift (red) and parallel velocity (orange) have zero magnitude and sum of all these terms is represented by Sum (dashed magenta).

varies sharply.

Under the guiding center limit, the electron moving with velocity \mathbf{v} gains energy through the work done by the electric field \mathbf{E} . The rate of energy gain is given by

$$\frac{dW}{dt} = q\mathbf{E}.(\mathbf{v}_{||} + \mathbf{v}_L + \mathbf{v}_E + \mathbf{v}_{cur} + \mathbf{v}_{\nabla B})$$
(13)

Figure 6 shows the rate of energy gain of an electron obtained from the test particle simulations a) Model and b) S1. The energy gain rate is expressed in the unit of $ev_A^2B_0/c$. The electric field for both Model and S1 is out-of-plane along z-direction. Hence, the $q\mathbf{E}.\mathbf{v}_{||}$ and $q\mathbf{E}.\mathbf{v}_{E}$ term vanishes (magnitude is zero in figure 6) as both $\mathbf{v}_{||}$ and \mathbf{v}_{E} are perpendicular to \mathbf{E} . The curvature

2742 (2024) 012015

doi:10.1088/1742-6596/2742/1/012015

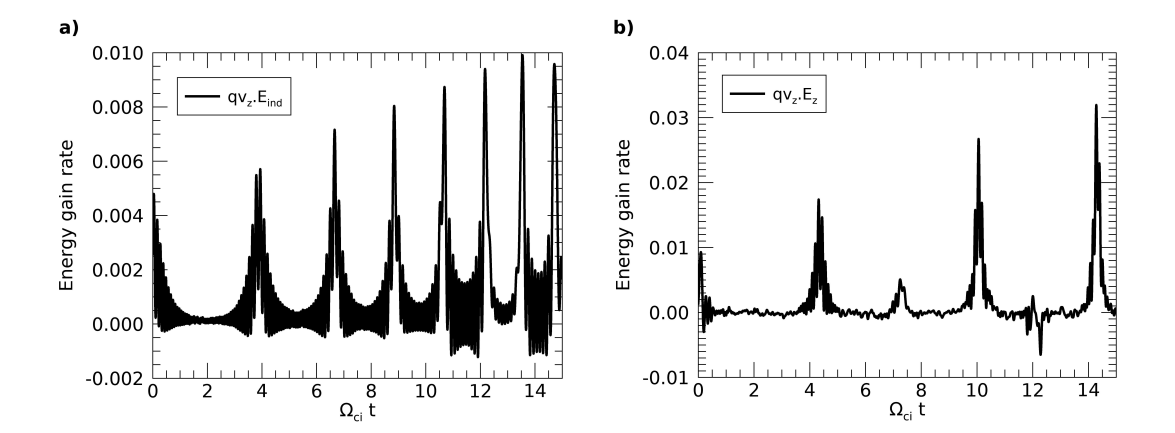


Figure 7. Electron's energy gain rate as a function of time from the test particle simulations a) Model and b) S1.

drift term dominates the electron's energy gain. Although gradient drift term is negligible, it decreases the electron's energy. The Larmor velocity also contributes in net increase of electron's energy. Therefore, their sum results in total energy gain which can also be seen from figure 7. The energy gain rate by the electron moving with velocity \mathbf{v} as the function of time is shown in figure 7. The rate of energy gain can be rewritten in the form

$$\frac{dW}{dt} = q\mathbf{E}.\mathbf{v} = qE_x v_x + qE_y v_y + qE_z v_z \tag{14}$$

Since the electric field is out-of-plane along z-direction, only the last term i.e. qE_zv_z in equation (14) contributes the electron's energy gain. The resemblance of energy gain rate due to various velocity terms between the Model and S1 in figure 6 and figure 7 suggests that the out-of-plane electric field \mathbf{E}_z is dominated by the inductive electric field generated by the contraction of the magnetic island and the energy gain is achieved through the work done by out-of-plane induced electric field.

5. Conclusion

The contraction of the magnetic island in the magnetic reconnection is modeled approximating an elliptical magnetic island together with an out-of-plane induced electric field. In the model, the particle's motion is nearly adiabatic and the released magnetic energy is converted into the kinetic energy of particles via the work done by the inductive electric field. The model predicts that the energy gain process is dominated by the curvature drift term and the prediction is verified by the test particle simulations on the fields generated by 2.5D particle-in-cell simulation showing electron acceleration via the contraction of a magnetic island.

6. Acknowledgments

The authors acknowledge partial support by NSF CAREER award 2144324 and NASA Heliophysics ECIP funding No. 80NSSC19K1106. The simulations were supported by the NASA High-End Computing (HEC) Program through the NASA Advanced Supercomputing (NAS) Division at Ames Research Center.

2742 (2024) 012015 doi:10.1088/1742-6596/2742/1/012015

7. References

- [1] Kopp R A and Pneuman G W 1976 Sol. Phys. **50** 85
- [2] Phan T D et al. 2000 Nature **404** 848
- [3] Lin R P et al. 2003 ApJ **595** L69
- $[4]\,$ Giannios D, Uzdensky, D A, and Begelman M C 2009 MNRAS $\bf 395\,$ L29
- [5] Hoshino M and Lyubarsky Y 2012 Space Sci. Rev. 173 521
- [6] Zhang H, Li X, Guo F and Giannios D 2018 ApJ **862** L25
- [7] Ji H, Yamada M, Hsu S and Kulsrud R 1998 Phys. Rev. Lett. 80 3256
- [8] Chien A et al. 2023 Nat. Phys. 19 254
- [9] Stenzel R L and Gekelman W 1984 Adv. Space Res. 4 459
- [10] Øieroset M, Lin R P, Phan T D, Larson D E and Bale S D 2002 Phys. Rev. Lett. 89 195001
- [11] Krucker S, Hudson H S, Glesener L, White S M, Masuda S, Wuelser J P and Lin R P 2010 ApJ 714 1108
- [12] Oka M et al. 2018 Space Sci. Rev. 214 82
- [13] Egedal J, Daughton W and Le A 2012 Nat. Phys. 8 321
- $[14]\,$ Uzdensky D A, Cerutti B and Begelman M C 2011 ApJ 737 L40
- [15] Drake J F, Swisdak M, Che H and Shay M A 2006 Nature 443 7111
- [16] Che H and Zank G P 2019 J. Phys.: Conf. Series 1332 012003
- [17] Majeski S and Hantao J 2023 Phys. Plasmas 30 042106
- [18] Che H and Zank G P 2020 ApJ 889 11
- [19] Che H, Zank G P and Benz A O 2021 ApJ 921 135
- [20] Zank G P, le Roux J A, Webb G M, Dosch A and Khabarova O 2014 ApJ 797 28
- [21] Dahlin J T, Drake J F and Swisdak M 2014 Phys. Plasmas 21 092304
- $[22]\,$ Li X, Guo F, Li Hui and Li G2017 ApJ ${\bf 843}$ 21
- [23] Li X, Guo F, and Li Hui 2019 ApJ 879 5
- [24] Guo F et. al 2019 ApJL **879** L23
- [25] Fermi E 1949 Phys. Rev. **75** 1169
- [26] Guidoni S E, DeVore C R, Karpen J T and Lynch B J 2016 ApJ 820 60
- [27] Dahlin J T 2020 Phy. Plasmas 27 100601
- [28] Daughton W, Roytershteyn V, Karimabadi H, Yin L, Albright B J, Bergen B and Bowers k J 2011 Nat. Phys. 7 539
- [29] Zeller A, Biskamp D, Drake J F, Rogers B N, Shay M A and Scholer M 2002 J. Geophys. Res.: Space Phys. 107 1230
- [30] Boris J P 1970 Relativistic plasma simulation-optimization of a hybrid code *Proceedings of the 4th Conference* on Numerical Simulation of Plasmas ed Boris J P and Shanny R A (Washington D.C.: Naval Research Laboratory) pp 3-67